Article

Prestress in Composite Polymer Gels as a Model of Extracellular Matrix

Alexandros Chremos[1,*], Jack F. Douglas[2] and Peter J. Basser[1], and Ferenc Horkay[1,*]

[1] Section on Quantitative Imaging and Tissue Sciences, *Eunice Kennedy Shriver* National Institute of Child Health and Human Development, National Institutes of Health, Bethesda, MD 20892, USA
[2] Materials Science and Engineering Division, National Institute of Standards and Technology, Gaithersburg, Maryland 20899, USA
* Correspondence: alexandros.chremos@nih.gov; horkayf@mail.nih.gov

Abstract: Articular cartilage is a composite hydrogel found in animal and human joints, which exhibits unique load-bearing properties that have been challenging to reproduce in synthetic materials and model in molecular dynamics (MD) simulations. We computationally investigate a composite hydrogel that mimics key functional properties of articular cartilage as a biomimetic model to investigate its unique load-bearing properties. Specifically, we find that the emergence of prestress in composite gels derives primarily from the stiffness of the polymer matrix and the asymmetry in the enthalpic interactions of the embedded particles and polymer matrix. Our MD simulations of the development of prestress agree qualitatively with osmotic pressure measurements observed in our model composite hydrogel material.

Keywords: gels; extracellular matrix; cartilage

Citation: Prestress in Composite Polymer Gels as a Model of Extracellular Matrix. *Gels* **2022**, *1*, 0. https://doi.org/

Received:
Accepted:
Published:

1. Introduction

Articular cartilage is a load-bearing composite hydrogel that caps the ends of bones in mammalian joints and is responsible for transmitting loads through the body. Articular cartilage primarily consists of water, ions,and the extracellular matrix (ECM), which is the main component responsible for the cartilage's mechanical properties. The ECM comprises a mesh of fibrous Type II collagen molecules and aggrecan is a bottlebrush-shaped proteoglycan (PG) polymer entrapped within the collagen matrix forming complexes with hyaluronic acid (HA) [1]. The organization of the macromolecular components in the ECM depends on the tissue type and its biological function (e.g., it is different in cartilage and brain) [2–5]. One biological function of articular cartilage is to ensure proper lubrication of joints during repetitive physical activity, such as walking. Another is to bear static and dynamic loads during activities like jumping and standing. Thus, the ECM in articular cartilage must expel fluid under compressive loading in physical activity, and recover its original shape and volume after unloading while minimizing joint wear [6,7]. Changes in the chemical composition and the organization of ECM's macromolecular constituents reduces the load-bearing ability of cartilage, an effect associated with osteoarthritis (OA) [8–11]. Irreversible articular cartilage degradation can occur by injury (e.g., traumatic OA), aging or inflammation (e.g., rheumatoid arthritis). Despite extensive research in characterizing articular cartilage's properties, no viable synthetic or naturally-derived cartilage implants can replicate its remarkable biological functions.

Knowledge of the structure and interactions of the components of cartilage is important for understanding the multiple biological functions of this structurally complex gel-like tissue, and for the development of therapeutic treatments for diseases, such as osteoarthritis, in which cartilage loses its functional properties [7,12,13]. For example, synovial fluid, which is rich in HA 'lubricates' joints, acts as a viscous liquid over relatively long timescales involved in slow joint movement and as an elastic material for rapid joint movement [1].

This may have implications for the ability of cartilage to undergo reversible deformation. Hardened cartilage makes moving the surrounding joints more difficult. The size of PG aggregates within ECM decreases with age [14]. This may occur as a result of a decrease in the available binding sites of the HA chain or as the result of damage to link proteins and the glycosaminoglycan chains. Aggregation may also affect pore size distribution and solute permeability [7]. In diseases such as osteoarthritis, the lubricating and load-bearing ability is reduced, however, the mechanisms that lead to the loss of cartilage's key biomechanical properties are still poorly understood [1,7,12,13].

Several attempts have been made to create gels with mechanical properties (stiffness, etc.) similar to articular cartilage [15–18]. Poly(vinyl alcohol) (PVA) is typically used because it is relatively insensitive to changes as a neutral polymer in the composition of the surrounding solution (e.g., salt concentration, pH). Chemically and/or physically cross-linked PVA gels are also widely used in biomedical applications [19–21]. However, the lack of viable synthetic cartilage implants not only necessitates the development of rational treatments to prevent joint damage, but also behooves us to obtain a deeper understanding of the physics and chemistry of cartilage-like gels to provide rational design principles to guide the development of functional cartilage implants. More generally, the development of such biomimetic cartilage-like materials and models, particularly through the use of polymer physics concepts, can provide a new fundamental understanding of the complex behaviors cartilage exhibits.

Horkay and Basser [22,23] recently proposed a novel composite hydrogel model of cartilage consisting of a poly(vinyl alcohol) (PVA) matrix, corresponding to the collagen matrix in articular cartilage, and cross-linked poly(acrylic acid) (PAA) microgel particles embedded within the PVA matrix, corresponding to the aggrecan/hyaluronic acid complex. The key feature of this composite hydrogel model is the development of "prestress," which is present even in the absence of any external loading, and which plays a critical role in governing the tissue's load-bearing ability. While this synthetic composite model exhibits a remarkable resemblance to articular cartilage in terms of load-bearing capabilities, a microscopic understanding based on polymer chemistry and the physics is required to explore the origin of the prestress. Besides providing a road-map to improve the performance of this composite hydrogel model in various applications (intervertebral disc spacers [24,25], shock absorbing materials [26], and sealants and caulks [27]), these compact gel particles entrapped in a network represent a new class of "squishy" materials whose study serves a larger scientific purpose while providing key insights into the normal function of cartilage and its dysfunction in abnormal development, disease, aging, and degeneration.

A similar strategy was used with the inclusion of cells in the extracellular matrix mimicked tissue mechanics in weak interacting gel systems [28]. The authors pointed out that particle inclusions can modify the elastic response of gel-like materials, which has important implications on tissue stiffness. They concluded that understanding the viscoelastic behavior of composite materials may shed light on the mechanisms by which tissue stiffness is altered in disease and to determine how changes in the mechanical microenvironment lead to cellular dysfunction. This finding is also important in the design of new biomaterials with physiologically relevant mechanical properties.

To gain a deeper understanding of the various physical and chemical molecular and macromolecular-scale processes governing the overall macroscopic functional properties of this material, we develop a minimal composite gel model to investigate the conditions and molecular parameters that govern the material behavior in aqueous solvent environments. To gain insights into the two primary components, the network and the embedded particles, we have developed models and methods to generate a wide range of gel-like structures ranging from compact [29] to open/fractal gel structures [30], as well as understanding the importance of attractions in the degree of swelling and osmotic properties [31]. In the current study, we describe a composite gel model composed of a polymer matrix containing embedded self-associating branched particles. Using this model, we investigated the conditions by which prestress reinforces this type of gel under isotropic compression.

This paper is organized as follows: Sec. 2 contains the details of the simulation methods and model. The experimental methodology is presented in Sec. 3. The results are presented in Sec. 4, where we investigate the influence of the extracellular matrix's topology and self-association of the embedded particles in the prestress of the composite gel. Finally, we draw our conclusions in Sec. 5.

2. Molecular Dynamics simulation methods and models

We employ a bead-spring model suspended in an implicit solvent, which was developed previously for studying the swelling behavior of linear polymer chains in solution and in melt conditions, and we have utilized it to describe the swelling of nanogel particles [31]. All the segments, polymer matrix and embedded particles, are assigned the same mass m, size σ, and strength of interaction ε; we assign ε and σ the units of energy and length, respectively.

The expression describing the non-bonded interactions operating between all pairs of beads contains three terms [32,33]. First is the Weeks-Chandler-Andersen (WCA) potential [34], which is a Lennard-Jones potential cut and shifted at the position of the minimum, $r_{\min} = 2^{1/6}\sigma$, to describe the purely repulsive interactions:

$$V_{\mathrm{WCA}}(r) = \begin{cases} 4\varepsilon\left[\left(\frac{\sigma}{r}\right)^{12} - \left(\frac{\sigma}{r}\right)^{6}\right] + \varepsilon & r \leq r_{\min} \\ 0 & r > r_{\min} \end{cases} \tag{1}$$

To represent the attractive interactions, the WCA potential is shifted in the range $0 \leq r \leq r_{\min}$ by a square-well (SW) potential,

$$V_{\mathrm{SW}}(r) = \begin{cases} -\lambda\varepsilon & 0 < r \leq r_{\min} \\ 0 & r > r_{\min} \end{cases} \tag{2}$$

where the well-depth parameter λ allows for tuning the effective monomer-monomer attractive interaction strength or the "solvent quality". To interpolate the potential smoothly between $-\lambda\varepsilon$ at $r = r_{\min}$ and 0 at a cut-off distance $r_{\mathrm{cut}} > r_{\min}$, we add the term

$$V_{\cos}(r) = \begin{cases} \frac{1}{2}\lambda\varepsilon\left[\cos\left(\alpha r^2 + \beta\right) - 1\right] & r_{\min} < r \leq r_{\mathrm{cut}} \\ 0 & r > r_{\mathrm{cut}} \end{cases} \tag{3}$$

α and β satisfy the conditions $\alpha r_{\min}^2 + \beta = \pi$ and $\alpha r_{\mathrm{cut}}^2 + \beta = 2\pi$. The cosine form of the potential also means that $\mathrm{d}V_{\cos}/\mathrm{d}r = 0$ at $r = r_{\mathrm{cut}}$. We choose $r_{\mathrm{cut}} = 3\sigma/2$, for which α and β become, $\alpha = \frac{4\pi}{9-4\sqrt[3]{2}}$ and $\beta = 2\pi - \frac{9}{4}\alpha$.

The final non-bonded potential is $V(r) = V_{\mathrm{WCA}} + V_{\mathrm{SW}}(r) + V_{\cos}(r)$, see Fig. 1a. The parameter λ controls the depth of the potential well at $r = r_{\min}$, and provides a convenient measure of the solvent quality. In a good solvent, the effective bead-bead interactions are purely repulsive; this corresponds to $\lambda = 0$. In a poor solvent, the bead-bead interactions are attractive, and this behavior can be modeled with $\lambda = 1$; the parameter λ also corresponds roughly to the Lennard-Jones potential well, which has been used frequently in the past in coarse-grained modeling of neutral polymers both in solution and in the melt [32,35,36]. The θ-solvent conditions for linear chains occur when $\lambda = 0.646$ [32].

The segments along a chain are connected with their neighbors via a stiff harmonic spring, $V_{\mathrm{H}}(r) = k(r - l_0)^2$, where $l_0 = 0.99\,\sigma$ is the equilibrium length of the spring, and $k = 1000\,\varepsilon/\sigma^2$ is the spring constant.

The polymer matrix has the same construction as a perfect compact gel composed of star polymers placed in a square or cubic lattice with their free ends bonded with the free ends of the neighboring stars. This model is discussed at length in recent publications [29–31]. The number of branched points (or star polymers) in each direction is labeled as N_x, N_y, and N_z [29]. The repeating branched structural unit of the polymer network studied here is identical to a regular star polymer. Other polymeric structures and/or other lattice morphologies could be utilized but these are outside the scope of the current study. A

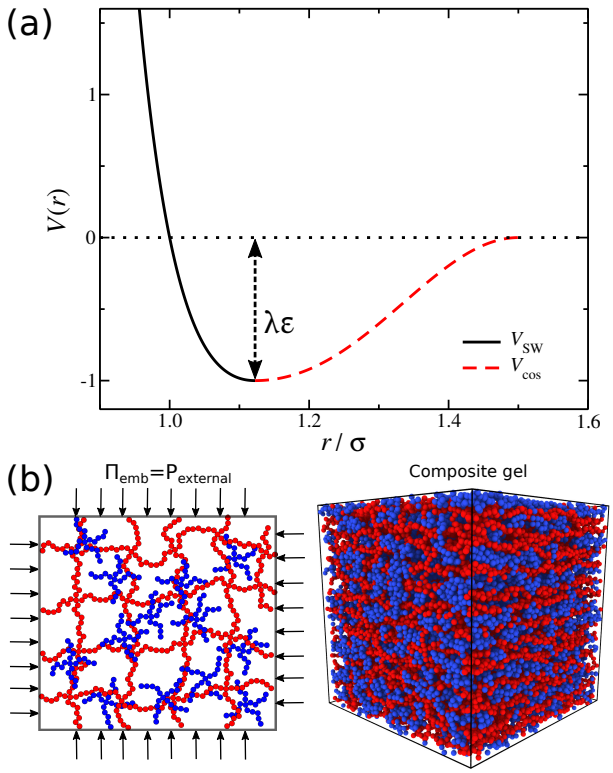

Figure 1. (a) The non-bonded, bead-bead interaction potential $V(r)$ with $\lambda = 1$, showing the contributions from $V_{\mathrm{WCA}}(r) + V_{\mathrm{SW}}(r)$ (black) and $V_{\cos}(r)$ (red). (b) Schematic and a screenshot of a composite gel model, where the polymer matrix is in red and the embedded gel particles are in blue. These systems are at equilibrium by having the osmotic pressure equal to external pressure.

regular star polymer has a core particle, which is connected with the free end of f_{mtx} chains (or arms) composed of M segments. Thus, the total number of interaction centers per star polymer is $M_{\mathrm{w,star}} = f_{\mathrm{mtx}}M + 1$. The molecular mass of the polymer matrix is $M_{\mathrm{w}} = (N_x N_y N_z) M_{\mathrm{w,star}}$. We use the quantity N_b to characterize the number of branched points in each direction. We focus on polymer matrix having $N_b = N_x = N_y = N_z$ and $f_{\mathrm{mtx}} = 4$ arms. The polymer matrix segment-segment interactions are purely repulsive with $\lambda_{\mathrm{mtx}} = 0$.

In the current study, the embedded particles are represented by a star polymer having $f_{\mathrm{emb}} = 4$ arms and arm length $M_{\mathrm{emb}} = 3$; the short length of the arms render this molecular structure to be highly spherically symmetric. The embedded particles are placed within the polymer matrix without overlaps, see Fig. 1b. The segment-segment interactions between the embedded particles is set by λ_{emb}. The segment-segment cross-interactions between the embedded particles and polymer matrix are set by λ_{cr} and unless stated otherwise $\lambda_{\mathrm{cr}} = 0$ for this study. The total number of embedded particles in the composite gel is such that the total number of segments of embedded particles, $n_{\mathrm{emb}} = N_{\mathrm{emb}}(f_{\mathrm{emb}}M_{\mathrm{emb}} + 1)$, is approximately equal to the number of segments composing the polymer matrix, $n_{\mathrm{mtx}} = N_{\mathrm{b}}^3(f_{\mathrm{mtx}}M_{\mathrm{mtx}} + 1)$, unless stated otherwise. In other words, we primiraly focus on composite gels having a composition $n_{\mathrm{emb}}/n_{\mathrm{mtx}} = 1$.

The systems were equilibrated at constant temperature $k_{\mathrm{B}}T/\varepsilon = 1.0$ and constant pressure maintained by a Nosé-Hoover thermostat and barostat. Typical simulations equilibrate for 5000 τ and data is accumulated over a 150 000 τ interval, where $\tau = \sigma(m/\varepsilon)^{1/2}$ is the MD time unit; the time step used was $\Delta t / \tau = 0.005$.

The osmotic pressure of the system is determined using the virial equation $\Pi_k = \rho kT + W/V$, where the internal virial W is calculated from the sum of a pairwise virial

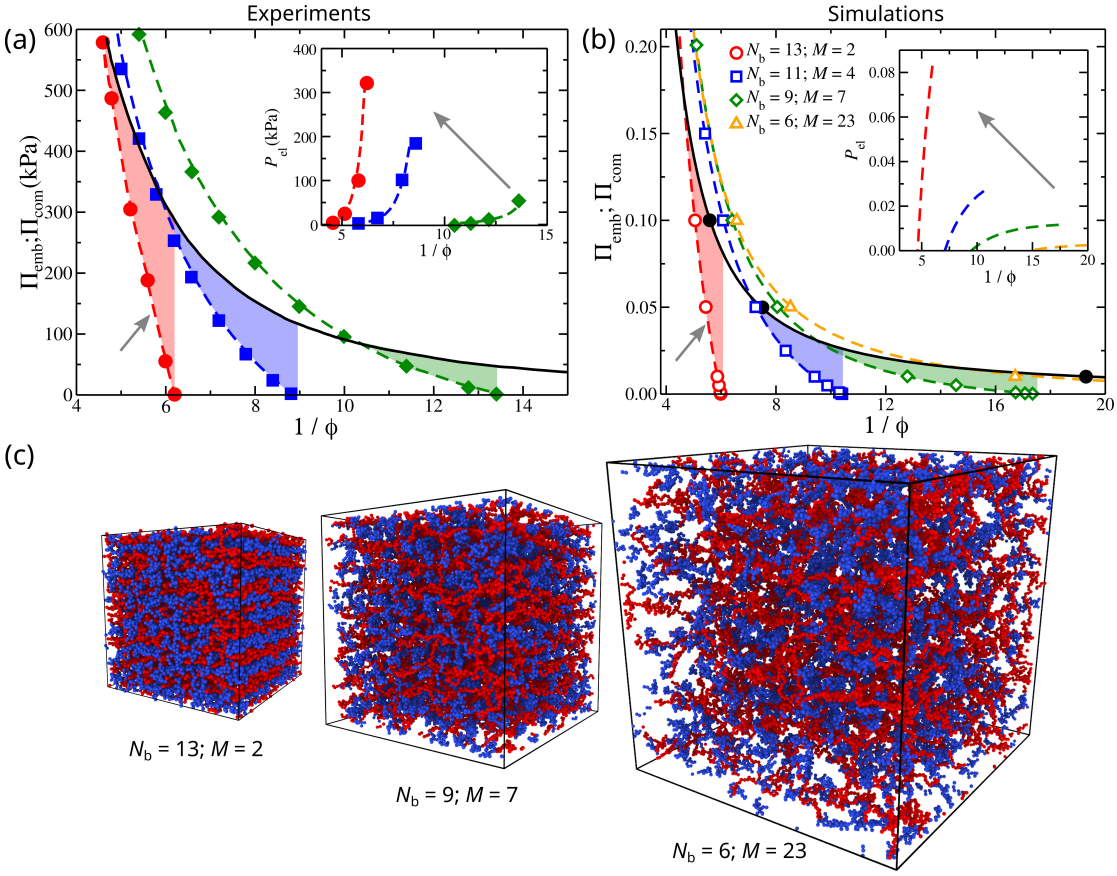

Figure 2. Osmotic pressure of composite gels, Π_{com}, in (a) experimental PVA/PAA varying network stiffness by changing the crosslinking density (dashed curves) and (b) simulation composite gel model having the strength of the attractions between them $\lambda_{emb} = 0.4$, as a function of the inverse of polymer fraction, $1/\phi$. In both (a) and (b) the osmotic pressure of embedded particles Π_{emb} is represented by the black continuous line, and in simulation results are represented by black filled circles. The highlighted regions outline the region at which P_{el} is calculated. The small arrows point to the composite gel that exhibits osmotic pressure similar to articular cartilage under physiological conditions [22]. Insets: prestress P_{el} as a function of $1/\phi$. The grey arrows at the insets of (a) and (b) point in the direction of increasing the polymer network stiffness. (c) Typical screenshots of composite gels having different gel architecture at $\Pi = 0.001$ and $\lambda_{emb} = 0.4$.

function $w(r_{ij}) = r_{ij} dU(r_{ij})/dr_{ij}$, and the index k corresponds to the different types of gel systems.

3. Preparation and characterization of composite PVA/PAA hydrogels

In the present study, we synthesized composite hydrogels using the procedure we have previously proposed [22]. We combine chemical cross-linking of PVA with partial crystallization induced by freeze thawing. PVA/PAA composite gels were prepared by dispersing PAA microgel particles in a PVA solution (1:1 ratio) prior to PVA cross-linking. The size of the PAA particles was in the range of 5 μm to 10 μm. Glutaraldehyde was used to cross-link the PVA molecules. The gels were equilibrated with 100 mol/m^3 NaCl solution. The swelling pressure of the gels Π_{com} was determined by an osmotic stress technique [37]. In this method gels enclosed in a dialysis bag are equilibrated with polymer solutions of known osmotic pressure [38]. At equilibrium, the concentrations of the gels and the polymer solutions are determined. This procedure yields the dependence of Π_{com} on the polymer volume fraction ϕ.

4. Results

At equilibrium, a swollen composite hydrogel coexists with the solvent by balancing two opposing forces. On the one hand, the gel swells due to the osmotic pressure of the polymer within the gel, Π_{mix}. In the absence of cross-links, the polymer chains are completely dissolved (in a good solvent) due to thermodynamic interactions between the polymer and solvent molecules. On the other hand, in the presence of cross-links, the osmotic pressure of the polymer is counterbalanced by the elastic pressure, Π_{el}, generated by the cross-links. Thus, we can formally decompose the osmotic pressure of the composite hydrogel, Π_{com}, into two components,

$$\Pi_{\text{com}} = \Pi_{\text{mix}} + \Pi_{\text{el}}. \tag{4}$$

At equilibrium $\Pi_{\text{com}} = 0$. In regular polymer gels, the elastic pressure, Π_{el}, decreases with an increasing degree of swelling, reflecting the cross-link density decrease. The prestress of the composite gel is defined as the difference of the pressure of the embedded particles (Π_{emb}) and the pressure of the composite gel,

$$P_{\text{el}} = \Pi_{\text{emb}} - \Pi_{\text{com}}. \tag{5}$$

Based on this definition, it is clear that at equilibrium the value of P_{el} will be $P_{\text{el,eq}} \approx \Pi_{\text{emb}}$. Thus, $P_{\text{el,eq}}$ is dominated by the pressure exerted by the embedded particles. For small, relatively simple embedded particles, the osmotic pressure will be well described by a virial equation of the form of $M_{\text{w}}\Pi_{\text{emb}}/\rho = 1 + B_2\rho + B_3\rho^2 + ...$, where B_2 and B_3 are the second and third virial coefficients. The osmotic pressure contributed by the polymer matrix can be described by Flory-Huggins expression [39],

$$\Pi_{\text{mix}} = -RT/V_1\left[\ln(1-\phi) + \phi + \chi_0\phi^2 + \chi_1\phi^3\right] \tag{6}$$

where V_1 is the partial volume of the solvent, ϕ is the volume fraction of the polymer, χ_0 and χ_1 are interaction parameters related to the second and third virial coefficients, R is the universal gas constant. The elastic contribution of the osmotic pressure is based on an expression that includes the intermolecular interactions in the gel discussed at length in Refs. 22,23,

$$\Pi_{\text{el}} = K_1\phi^{1/3} + K_2\phi^{4/3}, \tag{7}$$

where K_1 and K_2 are fitting parameters. We also note that the Flory-Huggins expression for describing the osmotic pressure of semi-dilute polymers and gels is only applicable for neutral systems. However, previous experimental studies and molecular dynamics simulations have indicated that the Flory-Huggins formalism is satisfactory for phenomenologically describing polyelectrolytes in the presence of added salt at concentrations relevant to physiological relevance and at high polymer concentrations where the mean-field theory would apply [40–42].

In Fig. 2a, we find that the experimental osmotic pressure is different between a solution of embedded particles and the composite gel. As discussed in previous studies [22,23], the osmotic pressure difference between these two systems is due to the gel's crosslinking and the influence of the filler on the composite gel's osmotic pressure. An increase in the gel's degree of crosslinking shiftes the osmotic pressure curves to smaller values of $1/\phi$, and increases the stiffness and the prestress of the composite gel, see inset of Fig. 2a.

Our model is in good qualitative agreement with experimental observations [22] of a composite hydrogel consisting of a poly(vinyl alcohol) (PVA) matrix encapsulating weakly cross-linked poly(acrylic acid) (PAA) microgel particles, see Fig. 2. We observe the same trends on how the mesh size of the polymer matrix influences the prestress of the composite gel, compare Figs. 2a and b. We note that an increase in crosslinking effectively reduces the mesh size in a gel. In particular, for a polymer matrices having the same total number of polymer matrix segments, then a decrease in the mesh size results in an increasing of

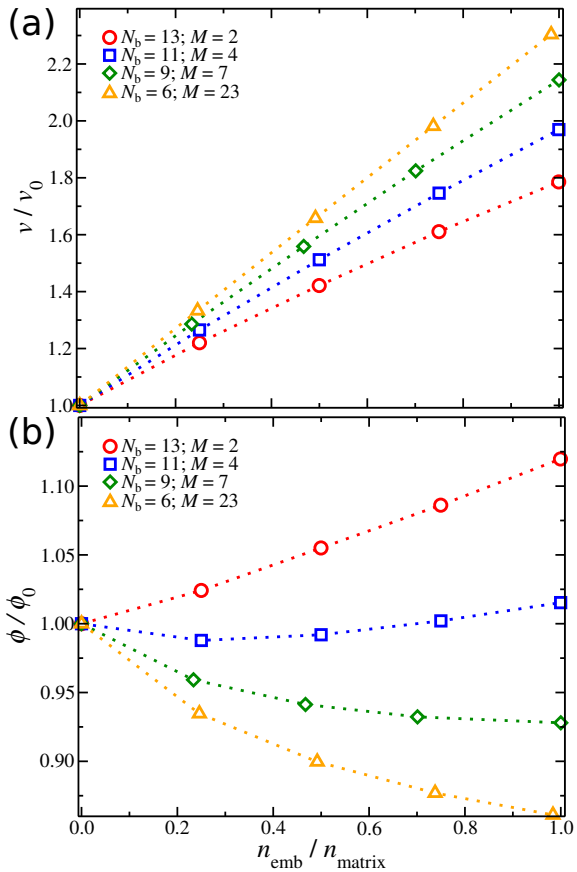

Figure 3. (a) Swelling of gel's volume normalized by the volume of a gel without embedded particles, v/v_0, as a function of the segmental composition defined as the ratio of the total number of embedded particles' segments over the total number of polymer matrix segments, $n_{\text{emb}}/n_{\text{mtx}}$, at fixed osmotic pressure of the composite gel, $\Pi_{\text{com}} = 0.01$. Results for different polymer matrices' chain length M are also presented. (b) Volume fraction normalized by the volume fraction of a gel without embedded particles, ϕ/ϕ_0, as a function of $n_{\text{emb}}/n_{\text{mtx}}$, at $\Pi_{\text{com}} = 0.01$. For both (a) and (b) the strength of association of embedded particles was $\lambda_{\text{emb}} = 0.4$.

the number of branched points in each direction while decreasing the chain length at same time. In other words, we increase the density of branching points in the gel structure by decreasing the mesh size. We find that decreasing the mesh size results in a decrease in the capacity of the polymer matrix to swell, which, in turn, decreases the value of $1/\phi$ at $\Pi_{\text{com}} = 0$, Fig. 2b. A smaller chain length means that the polymer matrix becomes stiffer by resisting volumetric changes, resulting in a rapid increase of Π_{com} with ϕ. A smaller mesh size also means the formation of smaller compartments in the polymer matrix for the embedded particles to occupy, which effectively creates frustration in the capacity of the embedded particles to associate with each other. Thus, the design of composite gels lies in the ability to control the distribution of contacts between the different species and the strength of their interactions. A key difference between our model and experimental observations is the concavity of the prestress curves, see insets of Fig. 2a & b, suggesting an additional layer of complexity is needed to capture this feature. Understanding the origin of this difference will be part of future work.

To understand the origin of the prestress in the composite gel, first, we need to examine the influence of the concentration of the embedded particles on the swelling of the extracellular matrix at fixed osmotic pressure conditions. In Fig. 3a, we calculate the degree of composite gel's volume swelling normalized by the volume of the gel without the embedded particles. As expected, the volume of the composite gel increases progressively

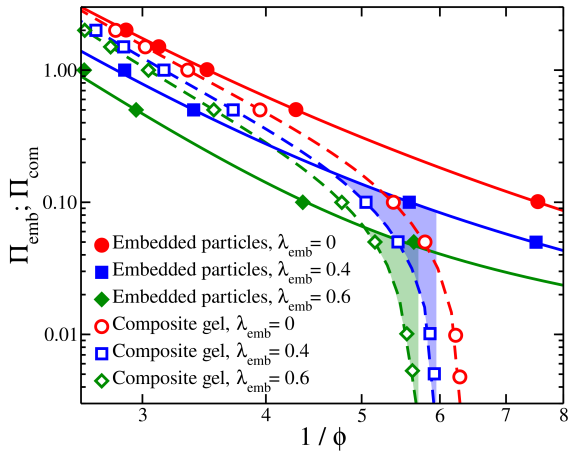

Figure 4. Osmotic pressure of composite gels Π_{com} (open symbols), with a polymer matrix having $N_b = 13$ and chain length $M = 2$, and osmotic pressure of embedded particles Π_{emb} (filled symbols) as a function of the inverse of polymer fraction $1/\phi$. The highlighted regimes outline the region at which the prestress is calculated. Results for different strengths of attractive interactions between the embedded particles are also presented.

as more embedded particles are included in the gel. However, the polymer matrices exhibit a faster volumetric swelling rate by increasing the chain length. In other words, shorter chain length in gels reduces the capacity of the gel to swell. This swelling effect has a non-trivial dependence on ϕ. We calculated the ratio of ϕ over the volume fraction of a gel without embedded particles, Fig. 3b. For $M > 4$, the volume fraction (of polymer matrix segments and embedded particles) decreases as the number of embedded particles in the gel increases. That's because the gel structure swells faster than the inclusion of embedded particles. For $M = 4$, we find that ϕ/ϕ_0 remains at approximately $\phi/\phi_0 \approx 1$, suggesting that at this chain length, the swelling rate is approximately the same with the increased number of embedded particles in the gel structure. For $M = 2$, the ratio ϕ/ϕ_0 progressively increases as the number of embedded particles increases, resulting in an increased packing of embedded particles in the polymer matrix. The behavior of ϕ/ϕ_0 is similar to the Hofmeister series of electrolyte solutions [43,44], where the embedded particles play the role of salt. The reduced capacity of the polymer matrix to sufficiently swell to accommodate the insertion of embedded particles within its gel structure results in the build-up of prestress.

The embedded particles play an important role in determining the properties of the composite gel. In our composite model, P_{el} progressively *increases* with $1/\phi$, thus leading to a maximum in P_{el}, see the insets of Figs. 2a & b. An increase in the strength of self-association between the embedded particles, λ_{emb}, decreases the height of osmotic pressure curves for both the composite gel and the embedded particle solution. However, an increase in λ_{emb} results in a more rapid decrease for Π_{emb}, see Fig. 4. This provides a mechanism for modulating the strength of attractive interactions between the embedded particles to control the value of $P_{el,eq}$ and the range of P_{el}. This illustrates the importance of physical interactions between the embedded particles and the polymer matrix (e.g., adsorption), playing a similar role as chemical crosslinks. Furthermore, the secondary structure formed by the self-association of the embedded particles (e.g., interparticle aggregates) may also affect gel stiffness. P_{el} decreases as $1/\phi$ decreases or alternatively reaches a plateau with $1/\phi$ when all interactions are strongly repulsive, see Fig. 5. Under these conditions, the behavior of P_{el} in our composite gel is no different from that of an ordinary gel. To avoid this behavior requires $\Pi_{emb} > \Pi_{com}$ at low densities/pressures and $\Pi_{emb} < \Pi_{com}$ at high densities/pressures, which implies that there is a point at which $\Pi_{emb} = \Pi_{com}$, resulting in $P_{el} = 0$. At high densities, the pressure is dominated by the segment-segment interactions,

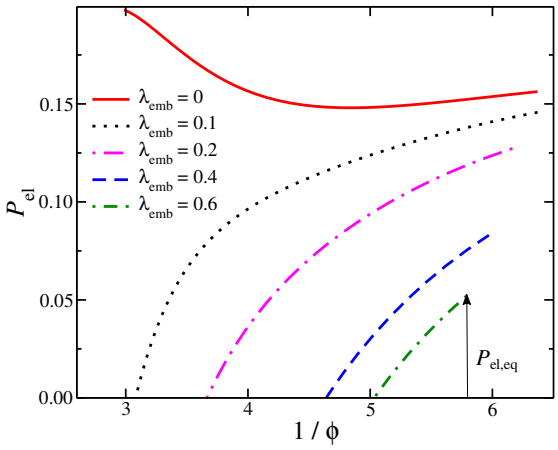

Figure 5. Prestress P_{el} of composite gels, with a polymer matrix having $N_b = 13$ and chain length $M = 2$, as a function of the inverse of the polymer fraction, $1/\phi$. Results at different strength of attractive interactions between the embedded particles are also presented. The arrow defines the value of prestress at equilibrium, $P_{el,eq}$, which occurs at $\Pi_{com} = 0$ for one of the systems.

which provide two potential approaches to making $\Pi_{emb} < \Pi_{com}$. The first approach is to increase the attractive interactions between the embedded particles. This type of interaction will decrease Π_{emb} and Π_{com} but its effect will be greater in Π_{emb} provided that the cross interactions between the embedded particle's segments and the segments of the polymer matrix remain fixed. This type of interaction effectively reduces the value of B_2 for the embedded particles. The second approach is based on increasing the attractive interactions between the embedded particles and the polymer matrix. This can be achieved by tuning non-dispersion type interactions, such as hydrogen bonding.

The influence of the attractive interactions between the embedded particles, regardless of whether these are self-interactions or cross interactions, does *not* further inflate the polymer matrix. Indeed, the maximum inflation of the polymer matrix occurs when all the interactions are purely repulsive, at which $P_{el,eq}$ is a minimum rather than a maximum. The attractive interactions enhance the association of the embedded particles, forming a loose network within the polymer matrix, which provides additional material rigidity under compression. We note that the attractions between the embedded particles need to be stronger than the attractions between the embedded particles and the polymer matrix to ensure that $\Pi_{emb} < \Pi_{com}$ for high pressures/densities. The results presented here are based on $\lambda_{cr} = 0$ (no cross-species attractions), but preliminary results (not shown here) support these observations. These lines of investigation will be part of future work.

The osmotic pressure of composite gels can be further tuned by varying the embedded particles' molecular mass. At low particle densities, the osmotic pressure of the embedded particles is close to the ideal behavior, $\Pi_{emb}/\rho \approx 1/M_w$. This suggests that at equilibrium $\Pi_{com} \approx 0$ and according to Eq. 5, then $P_{el,eq}$ increases by having embedded particles of smaller molecular mass, thus $P_{el,eq} \sim \rho/M_w$ at fixed density. The molecular mass and the strength of attractions of the embedded particles determine $P_{el,eq}$. As the complexity of the model increases, such as by the inclusion of hydration, electrostatic, and pH effects, as well as entanglements, we anticipate that there will be more mechanisms available to tune the prestress behavior of these composite gels. The present work is just a first step in the modeling of these complex gels and additional features such as charged monomers, hydration of the chain backbone and the monomers and counter-ions, etc. so that we can address sthe apparent difference in the concavity between the prestress curves between experimental and simulation results. These extensions will require ongoing computational effort and additional measurements to validate the theory.

The optimal crosslink density of the embedded particles is not obvious. Weakly crosslinked PAA exhibits high swelling pressure, eventually destabilizing and destroying

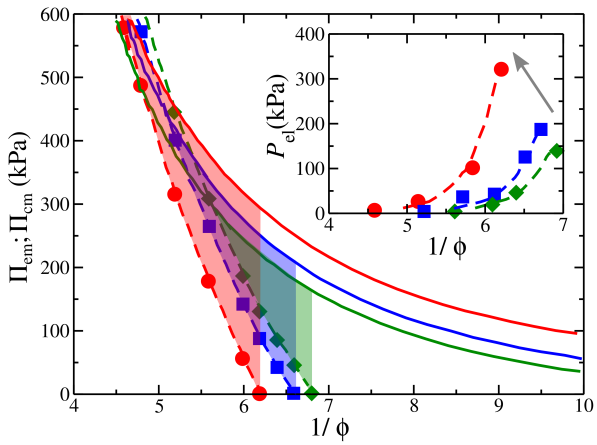

Figure 6. Experimental osmotic pressure of PVA/PAA composite gels containing PAA particles of varying nominal cross-link densities (dashed lines) and (continuous lines) PAA gels with varying cross-linking densities (high to low from left to right). The highlighted regions outline the region at which P_{el} is calculated. Inset: prestress P_{el} as a function of the inverse of polymer fraction, $1/\phi$. The grey arrow point in the direction of increasing the polymer network stiffness.

the PVA matrix. On the other hand, the limited swelling of densely crosslinked PAA particles may not be sufficient to inflate the PVA gel. This suggests that a composition exists between these two extremes of weak and highly-dense crosslinking where the composite gel exhibits the optimum mechanical properties. Increasing the cross-linking density of the embedded PAA gel particles also influences the prestress, see Fig. 6. Increasing the crosslink density progressively reduces the swelling of the embedded particles and shifts the Π_{com} *vs.* $1/\phi$ curves toward lower swelling pressures.

5. Conclusions

In our study, we propose a general model of composite gels that exhibit mechanical properties of high compressive load-bearing ability. This is achieved by creating a polymer matrix having a small mesh size and embedding in it self-associating small particles. A small mesh size polymer matrix has a large number of branched points that reinfoce the polymer matrix, while the embedded particles inflate the volume of the polymer matrix. Combining these features results in new high-strength composite gel materials. In our framework, it becomes possible to tune the molecular parameters of the two components to create composite gels that mimic the biological function of articular cartilage [22,23]. Overall, we establish a minimal composite gel model that reproduces the behavior of high-strength composite gel materials for many potential applications. Our findings provide scientific insight into the molecular origin of the interactions between and among the different compartments and their role in determining key material properties in this class of materials.

Author Contributions: Conceptualization, J.F.D. and A.C.; methodology, A.C.; software, A.C.; validation, A.C.; investigation, A.C.; writing—original draft preparation, A.C.; writing—review and editing, all authors; visualization, A.C.; supervision, F.H.; funding acquisition, P.J.B. All authors have read and agreed to the published version of the manuscript.".

Funding: This research was supported by the Intramural Research Program of the *Eunice Kennedy Shriver* National Institute of Child Health and Human Development, NIH.

Conflicts of Interest: The authors declare no conflict of interest.

References

1. Buckwalter, J.A.; Mankin, H.J. Articular cartilage: part I. *J. Bone Jt. Surg.* **1997**, *79*, 600–611.

2. Ruoslahti, E. Brain extracellular matrix. *Glycobiology* **1996**, *6*, 489–492.
3. Novak, U.; Kaye, A.H. Extracellular matrix and the brain: components and function. *J. Clin. Neurosci.* **2000**, *7*, 280–290.
4. Frantz, C.; Stewart, K.M.; Weaver, V.M. The extracellular matrix at a glance. *J. Cell Sci.* **2010**, *123*, 4195–4200.
5. Bowers, S.L.; Banerjee, I.; Baudino, T.A. The extracellular matrix: at the center of it all. *J. Mol. Cell. Cardiol.* **2010**, *48*, 474–482.
6. Maroudas, A. Balance between swelling pressure and collagen tension in normal and degenerate cartilage. *Nature* **1976**, *260*, 808–809.
7. Sophia Fox, A.J.; Bedi, A.; Rodeo, S.A. The basic science of articular cartilage: structure, composition, and function. *Sports Health* **2009**, *1*, 461–468.
8. Buckwalter, J.A.; Mankin, H.J.; Grodzinsky, A.J. Articular cartilage and osteoarthritis. *Instr. Course Lect.* **2005**, *54*, 465.
9. Pearle, A.D.; Warren, R.F.; Rodeo, S.A. Basic science of articular cartilage and osteoarthritis. *Clin. Sports Med.* **2005**, *24*, 1–12.
10. Martel-Pelletier, J.; Boileau, C.; Pelletier, J.P.; Roughley, P.J. Cartilage in normal and osteoarthritis conditions. *Best Pract. Res.: Clin. Rheumatol.* **2008**, *22*, 351–384.
11. Heinegard, D.; Saxne, T. The role of the cartilage matrix in osteoarthritis. *Nat. Rev. Rheumatol.* **2011**, *7*, 50–56.
12. Mow, V.C.; Hung, C.T. Biomechanics of Articular Cartilage. In *Basic Biomechanics of the Musculoskeletal System*; Nordin, M.; Frankel, V.H., Eds.; Lippincott Lea & Feviger: Philadelphia, PA, 2001; pp. 60–101.
13. Lu, X.L.; Mow, V.C. Biomechanics of articular cartilage and determination of material properties. *Med. Sci. Sports Exerc.* **2008**, *40*, 193–199.
14. Rahmati, M.; Nalesso, G.; Mobasheri, A.; Mozafari, M. Aging and osteoarthritis: central role of the extracellular matrix. *Ageing Res. Rev.* **2017**, *40*, 20–30.
15. Grant, C.; Twigg, P.; Egan, A.; Moody, A.; Smith, A.; Eagland, D.; Crowther, N.; Britland, S. Poly(vinyl alcohol) hydrogel as a biocompatible viscoelastic mimetic for articular cartilage. *Biotechnol. Prog.* **2006**, *22*, 1400–1406.
16. Ma, R.; Xiong, D.; Miao, F.; Zhang, J.; Peng, Y. Novel PVP/PVA hydrogels for articular cartilage replacement. *Mater. Sci. Eng. C* **2009**, *29*, 1979–1983.
17. Hassan, C.; Peppas, N.A. Structure and applications of poly(vinyl alcohol) hydrogels produced by conventional crosslinking or by freezing/thawing methods. *Adv. Polym. Sci.* **2000**, *153*, 37–66.
18. Horkay, F.; Burchard, W.; Geissler, E.; Hecht, A.M. Termodynamic properties of poly(vinyl alcohol) and poly(vinyl alcohol-vinyl acetate) hydrogels. *Macromolecules* **1993**, *26*, 1296–1303.
19. Allen, M.J.; J. E. Schoonmaker, T.W.B.; Williams, P.F.; Higham, P.A.; Yuan, H.A. Preclinical evaluation of a poly(vinyl alcohol) hydrogel implant as a replacement for the nucleus pulposus. *Spine* **2004**, *29*, 515–523.
20. Kobayashi, M.; Chang, Y.; Oka, M. A two year in vivo study of polyvinyl alcohol hydrogel (PVA-H) artifcial meniscus. *Biomaterials* **2005**, *26*, 3243–3248.
21. Holloway, J.L.; Lowman, A.M.; Palmese, G.R. Mechanical evaluation of poly(vinyl alcohol) based fibrous composites as biomaterials for meniscal tissue replacement. *Acta Biomater.* **2010**, *6*, 4716–4724.
22. Horkay, F.; Basser, P.J. Composite hydrogel model of cartilage predicts its load-bearing ability. *Sci. Rep.* **2020**, *10*, 1–7.
23. Horkay, F.; Basser, P.J. Hydrogel composite mimics biological tissues. *Soft Matter* **2022**, *18*, 4414–4426.
24. Langrana, N.A.; Parsons, J.R.; Lee, C.K.; Vuono-Hawkins, M.; Yang, S.W.; Alexander, H. Materials and design concepts for an intervertebral disc spacer. I. Fiber-reinforced composite design. *Journal of Applied Biomaterials* **1994**, *5*, 125–132.
25. Bao, Q.B.; Mccullen, G.M.; Higham, P.A.; Dumbleton, J.H.; Yuan, H.A. The artificial disc: theory, design and materials. *Biomaterials* **1996**, *17*, 1157–1167.
26. Calvert, P. Hydrogels for soft machines. *Adv. Mater.* **2009**, *21*, 743–756.
27. Prane, J.W.; Elias, M.; Redman, R. Sealants and caulks. In *In Handbook of adhesives*; Springer: Boston, MA, 1990; pp. 611–640.
28. van Oosten, A.S.; Chen, X.; Chin, L.; Cruz, K.; Patteson, A.E.; Pogoda, K.; Shenoy, V.B.; Janmey, P.A. Emergence of tissue-like mechanics from fibrous networks confined by close-packed cells. *Nature* **2019**, *573*, 96–101.
29. Chremos, A.; Douglas, J.F.; Horkay, F. Structure and conformational properties of ideal nanogel particles in athermal solutions. *J. Chem. Phys.* **2021**, *155*, 134905.
30. Chremos, A.; Douglas, J.F.; Horkay, F. Influence of network defects on the conformational structure of nanogel particles: From "closed compact" to "open fractal" nanogel particles. *J. Chem. Phys.* **2022**, *156*, 094903.
31. Chremos, A.; Douglas, J.F.; Basser, P.; Horkay, F. Molecular Dynamics Study of the Swelling and Osmotic Properties of Compact Nanogel Particles. *Soft Matter; in press* **2022**.
32. Soddemann, T.; Dünweg, B.; Kremer, K. A generic computer model for amphiphilic systems. *EPJ E* **2001**, *6*, 409–419.
33. Steinhauser, M.O. A molecular dynamics study on universal properties of polymer chains in different solvent qualities. Part I. A review of linear chain properties. *J. Chem. Phys.* **2005**, *122*, 094901.
34. Weeks, J.D.; Chandler, D.; Andersen, H.C. Role of repulsive forces in determining the equilibrium structure of simple liquids. *J. Chem. Phys.* **1971**, *54*, 5237–5247.
35. Chremos, A.; Glynos, E.; Koutsos, V.; Camp, P.J. Adsorption and self-assembly of linear polymers on surfaces: a computer simulation study. *Soft Matter* **2008**, *5*, 637–645.
36. Chremos, A.; Glynos, E.; Koutsos, V.; Camp, P.J. Adsorption of star polymers: computer simulations. *Soft Matter* **2010**, *6*, 1483–1493.

37. Horkay, F.; Zrinyi, M. Studies on mechanical and swelling behavior of polymer networks based on the scaling concept, 4. Extension of the scaling approach for gels swollen to equilibrium in a diluent of arbitrary activity. *Macromolecules* **1982**, *15*, 1306–1310.
38. Vink, H. Precision measurements of osmotic pressure in concentrated polymer solutions. *Eur. Polym. J.* **1971**, *7*, 1411–1419.
39. Horkay, F.; Tasaki, I.; Basser, P.J. Osmotic swelling of polyelectrolyte hydrogels in physiological salt solutions. *Biomacromolecules* **2000**, *1*, 84–90.
40. Nicodemus, G.D.; Bryant, S.J. Cell encapsulation in biodegradable hydrogels for tissue engineering applications. *Tissue Eng. Part B* **2008**, *14*, 149–165.
41. Horkay, F.; Basser, P.J.; Hecht, A.M.; Geissler, E. Structural investigations of a neutralized polyelectrolyte gel and an associating neutral hydrogel. *Biomacromolecules* **2005**, *46*, 4242–4247.
42. Horkay, F.; Basser, P.J. Osmotic observations on chemically cross-linked DNA gels in physiological salt solutions. *Biomacromolecules* **2004**, *5*, 232–237.
43. Andreev, M.; Chremos, A.; de Pablo, J.; Doulgas, J.F. Coarse-grained model of the dynamics of electrolyte solutions. *J. Phys. Chem. B* **2017**, *121*, 8195–8202.
44. Andreev, M.; de Pablo, J.; Chremos, A.; Doulgas, J.F. Influence of ion solvation on the properties of electrolyte solutions. *J. Phys. Chem. B* **2018**, *122*, 4029–4034.